Supporting Information

Concentration enrichment, separation, and cation exchange in nanoliter-scale water-in-oil droplets

Sungu Kim[1,2], Baskar Ganapathysubramanian[1], Robbyn K. Anand[2]*

[1]Department of Mechanical Engineering, Iowa State University, 2043 Black Engineering, 2529 Union Drive, Ames, IA 50011-2030
[2]Department of Chemistry, Iowa State University, 1605 Gilman Hall, 2415 Osborn Drive, Ames, IA 50011-1021

The integration of concentration enrichment schemes with droplet microfluidics has been previously undertaken to accomplish two goals: (1) to physically isolate locally enriched species from a bulk solution (enrichment prior to droplet formation), and (2) to enhance the detection of a target species present in a droplet (enrichment after droplet formation). **Table S1** summarizes approaches that accomplish these goals.

Table S1. Approaches that combine droplet microfluidics with concentration enrichment.

First Author	*Enrichment before/after droplet formation*	*Full contents of droplet enriched?*	*Enrichment mechanism*
Yu [1]	Before	N/A	ICP-enriched BSA sent to droplet generator
Chen [2]	Before	N/A	ICP-enriched cell lysate sent to droplet generator
Sanghavi [3]	After	No	Part of droplet enriched by ICP in nanochannel
Petersson [4]	After	Yes	Active evaporation of droplet volume
He [5]	After	Yes	Passive evaporation of droplet volume
Park [6]	After	Yes	Traveling surface acoustic waves enrich beads
This study	After	Yes	ICP of the entire contents of each droplet, spatial separation of droplet components, and cation exchange

In two of these reports, target species are enriched and separated into focused bands prior to subsequent encapsulation into droplets. This strategy was employed to 'lock in' the 10^4-fold enrichment of dye-linked bovine serum albumin (BSA) [1] and to accomplish a 10-fold reduction in assay time following the 16-fold enrichment of matrix metalloproteinases (MMPs) from diluted cellular supernatant prior to droplet encapsulation [2]. To achieve enrichment of solutes after a sample is encapsulated into droplets, Sanghavi et al. demonstrated the extraction of analytes from droplets by microdialysis and their subsequent enrichment by ICP in

nanochannels [3]. This approach allows sampling and enhanced detection of a limited portion of the droplet contents. In-droplet enrichment of solutes has been accomplished by evaporation [4,5], and more recently, traveling acoustic waves (TSAWs) were employed to enrich polystyrene beads prior to droplet splitting at a Y-junction [6]. This overview of related techniques highlights the need for a method that is capable of enrichment of a target species from the entire volume of a droplet.

Device fabrication. The device that was utilized for in-droplet ICP was constructed from a glass substrate, onto which two parallel thin film Nafion membranes were patterned, aligned with an upper PDMS monolith that defined three independent microfluidic channels. The membranes were flow-patterned on the glass substrate as follows. First, a PDMS monolith (green, **Scheme S1a**) was caste-molded on a Si wafer patterned with SU-8 2025. The PDMS was imprinted with two channels, spaced 300 μm apart measuring 6.0 mm long, 400 μm wide, and 25.0 μm tall with a 1.0 mm-diameter inlet and outlet. Second, a 25 mm x 25 mm x 1 mm glass slide was cleaned in an alkaline solution (NH_4OH:H_2O:H_2O_2, 1:1:1, at 60 ℃ for 10 min) followed by rinsing with d.d.i. water, ethanol, drying with N_2, and 60 s exposure to O_2 plasma. Third, the PDMS monolith was reversibly sealed to the glass slide. Nafion resin was pipetted on top of the inlet of each channel and then pulled through by suction applied to the outlet (**Scheme S1b**). Then, the glass slide was baked at 95 ℃ for 10 min on a hot plate to cure the Nafion (**Scheme S1c**). While curing, the Nafion shrinks to its final thickness of 2-8 μm. The PDMS channels used to pattern the membranes was peeled away leaving cured Nafion on the slide glass.

Separately, a PDMS monolith defining three microchannels (orange, **Scheme S1a**) was fabricated by soft lithography from a SU-8 2050 patterned Si wafer. The central ‘main microchannel’ was 10.0 mm long, 500 μm wide, and 50.0 μm tall spanning a 1.0 mm-diameter inlet and outlet. The two flanking auxiliary channels were separated from the main channel by a 250 μm-thick wall and had were 5.0 mm long, 500 μm wide, and 50.0 μm tall with 4.0 mm-diameter reservoirs at each end. This PDMS monolith was exposed to an O_2 plasma for 60 s. Immediately after plasma treatment, these three microchannels were aligned on top of the membranes. Finally, the device was baked at 95 ℃ for 10 min in an oven (**Scheme 1d**). Note that channels were aligned parallel to the membranes and centered on them such that each membrane spanned the wall between an auxiliary channel and the main channel. Finally, the main channel was filled with the oil phase, and the auxiliary channels were filled with an aqueous electrolyte (phosphate buffer) with concentration matched to that of the droplets described for each experiment in the *Results and Discussion*.

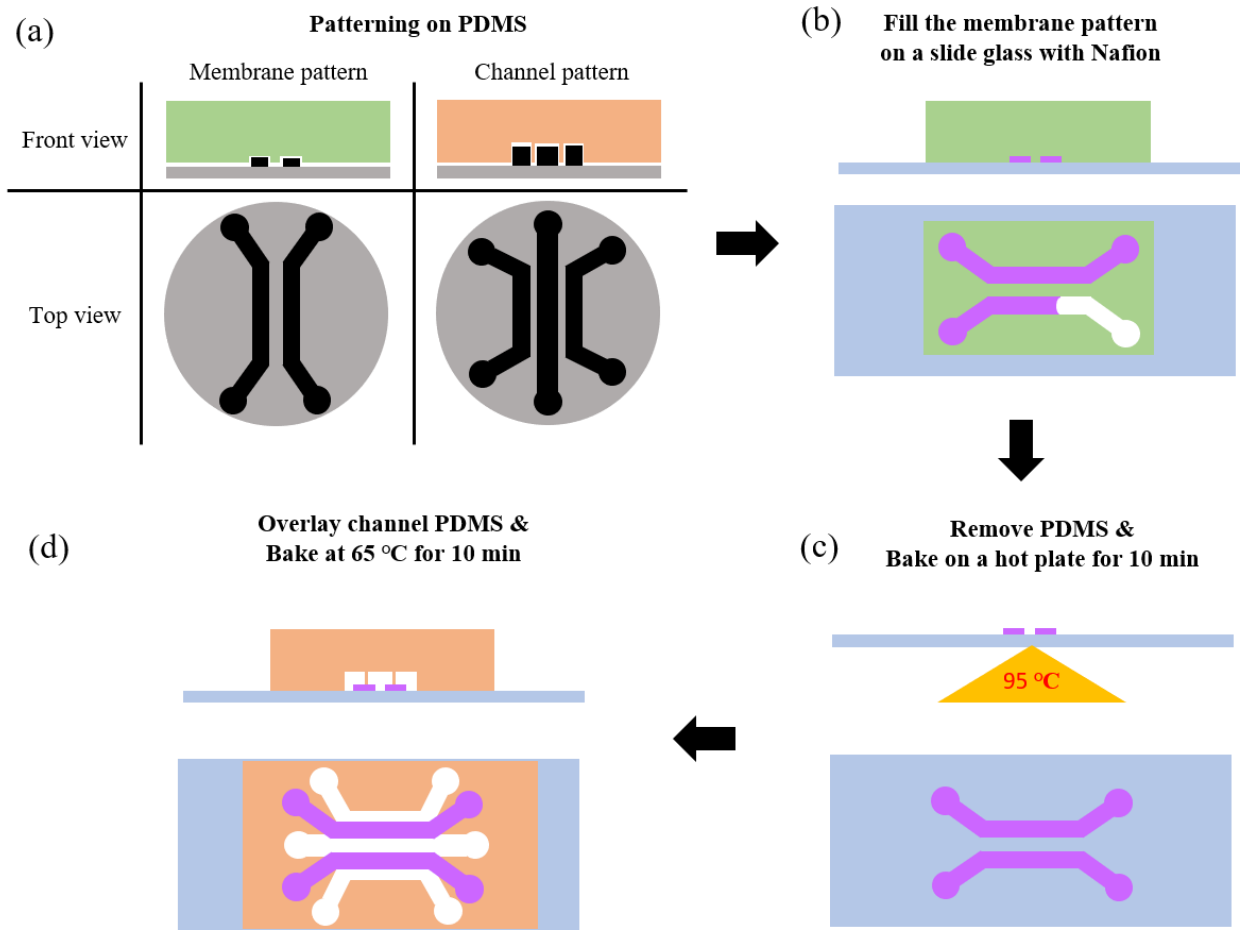

Scheme S1. Device preparation. Pattern membrane and channels on PDMS from a silicon wafer (a). Place the membrane PDMS on the slide glass, then, inject Nafion solution through punch holes (b). Bake at 95 °C for 10 min to cure Nafion on a hot plate and remove the PDMS (c). Align the channel PDMS chip on the membrane (d).

Conservation of mass in droplets. The W/O interface and cation selective membrane isolate anionic analytes inside a droplet. This isolation allows enrichment without loss of analyte. The variation in integrated fluorescence intensity across the droplet, δ_t, was evaluated using the following equation.

$$\delta_t = \frac{\int_{\Omega_D} I_t \, \partial\Omega_D - \int_{\Omega_D} I_0 \partial\Omega_D}{\int_{\Omega_D} I_0 \, \partial\Omega_D} \approx \frac{\sum_{i\in\Omega_D} I_{t,i} - \sum_{i\in\Omega_D} I_{0,i}}{\sum_{i\in\Omega_D} I_{0,i}} \qquad (1)$$

Here, I_t, I_0, and Ω_D are the local intensity at time t, the local intensity at $t = 0$ s, and the projected area of the droplet in the image. Subscript i represents the pixel index. **Figure S1** shows the maximum δ_t, expressed as a percentage, at several voltage biases. The variations of droplet intensity were minute with the average value 3.8±0.3%. This small variation confirms that the majority of the analyte was confined to the droplets during the enrichment.

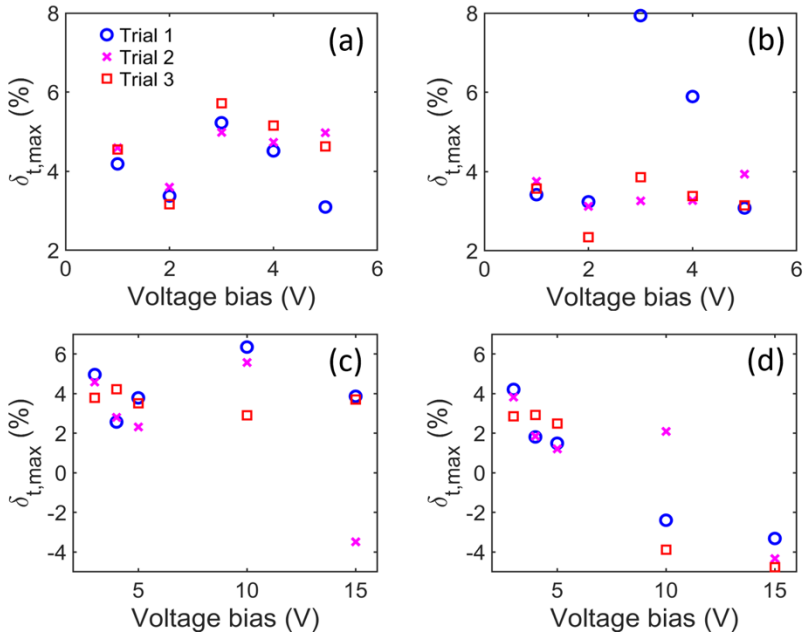

Fig. S1. The maximum percent change in integrated fluorescence, δ_t, during the enrichment of stationary droplets at several voltages; three trials each at (a) 1.0 mM phosphate buffer, 22.3 nL droplet, (b) 1.0 mM phosphate buffer, 3.9 nL droplet, (c) 10.0 mM phosphate buffer, 6.4 nL droplet, and (a) 10.0 mM phosphate buffer, 4.6 nL droplet. The negligible variation during the enrichment ensures the majority of analytes were confined inside the droplets. The mean maximum variation was 3.8±0.3%.

Evaluation of enrichment factor (EF) and normalized IDZ size. EF is the ratio between the maximum enriched concentration and the original concentration. EF was evaluated by dividing the maximum intensity in the droplet by the average droplet intensity, obtained prior to initiation of a voltage bias, where, N_D is the number of pixels in the droplet.

$$EF = \frac{\max\limits_{i \in \Omega_D} I_i}{\sum_{i \in \Omega_D} I_{0,i}/N_D} \qquad (2)$$

To evaluate the normalized IDZ size, the number of pixels in the IDZ region, N_{IDZ}, was divided by the number of pixels in the entire droplet as expressed below.

$$\frac{N_{IDZ}}{N_D} \qquad (3)$$

Intensity profile along the droplet centerline during ICP. Figures S2-S5 show the temporal evolution of the fluorescence intensity profile along the droplet centerline that lies perpendicular

to the channel axis. Each figure comprises data for a distinct droplet volume and composition. Plots (a-e) within a figure differ by voltage. Note that the location of the maximum fluorescence intensity within a droplet is frequently not located on the centerline; therefore, the intensity profiles plotted here may not reflect the calculated EF.

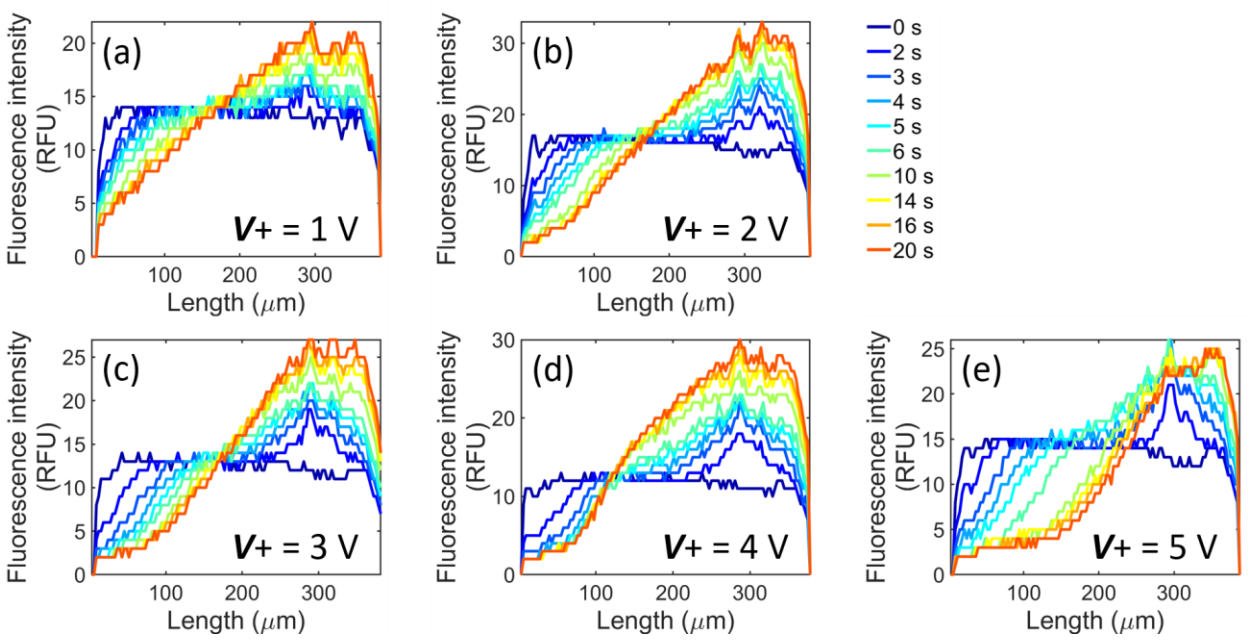

Fig. S2. Temporal evolution of the fluorescence intensity profile along the droplet centerline of a 22.3 nL droplet containing 1.0 mM phosphate buffer and 10.0 μM $BODIPY^{2-}$. The applied voltage bias was (a) 1 V, (b) 2 V, (c) 3 V, (d) 4 V, and (e) 5 V.

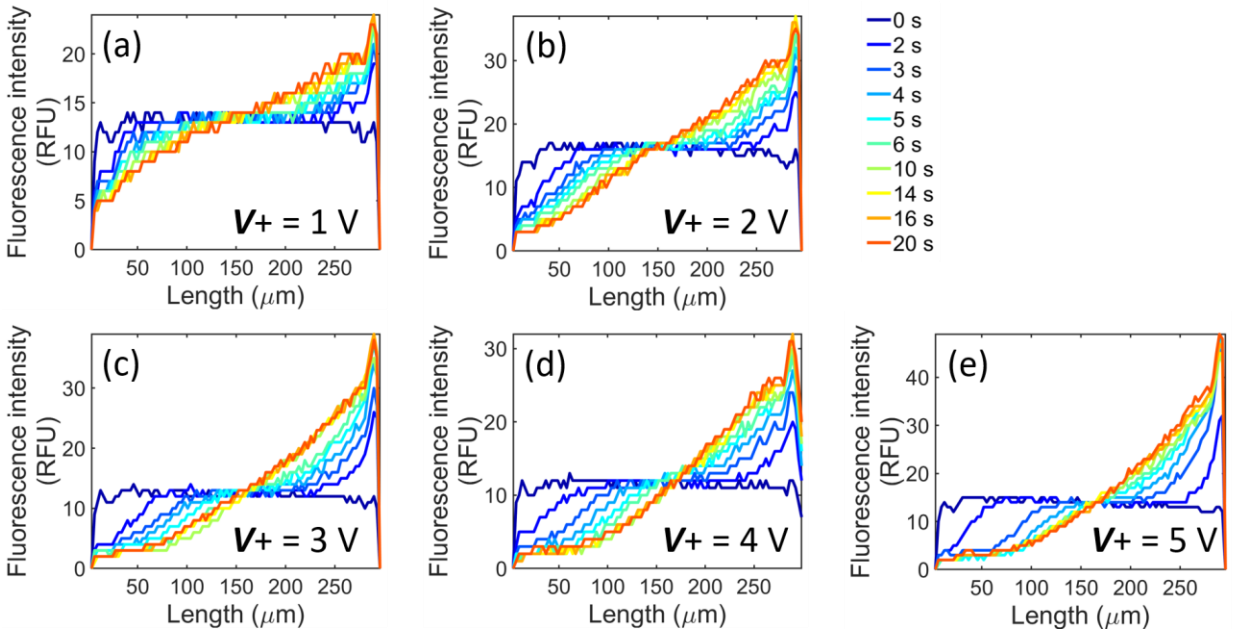

Fig. S3. Temporal evolution of the fluorescence intensity profile along the droplet centerline of a 3.9 nL droplet containing 1.0 mM phosphate buffer and 10.0 μM $BODIPY^{2-}$. The applied voltage bias was (a) 1 V, (b) 2 V, (c) 3 V, (d) 4 V, and (e) 5 V.

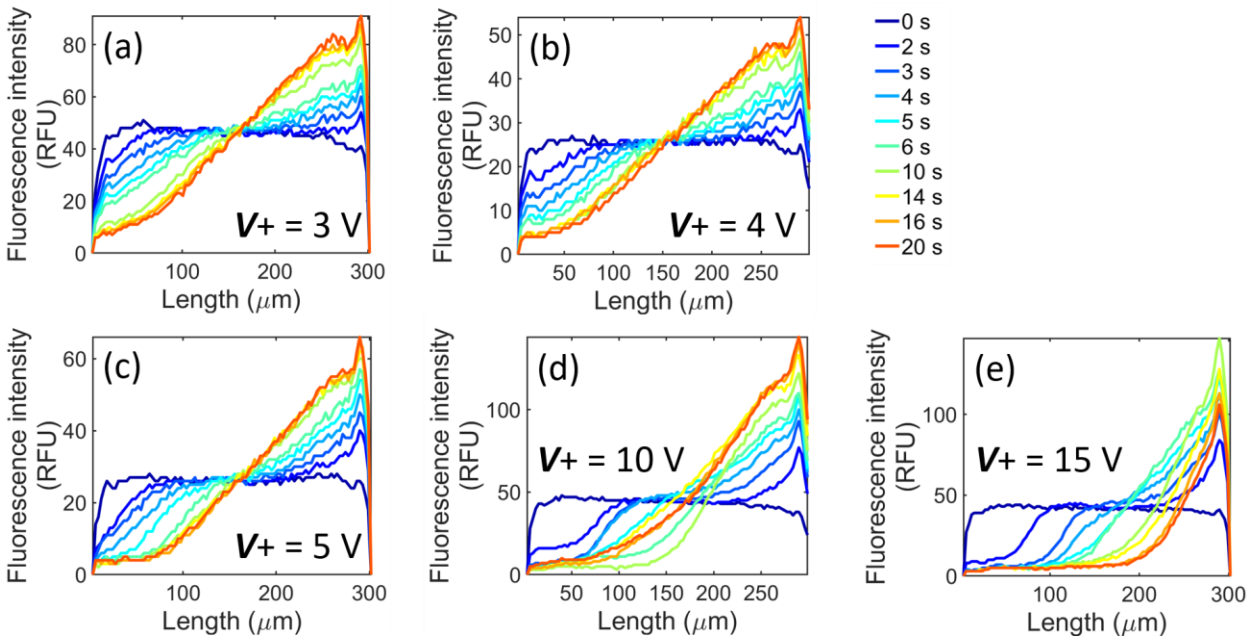

Fig. S4. Temporal evolution of the fluorescence intensity profile along the droplet centerline of a 6.4 nL droplet containing 10.0 mM phosphate buffer and 10.0 μM $BODIPY^{2-}$. The voltage bias was (a) 3 V, (b) 4 V, (c) 5 V, (d) 10 V, and (e) 15 V.

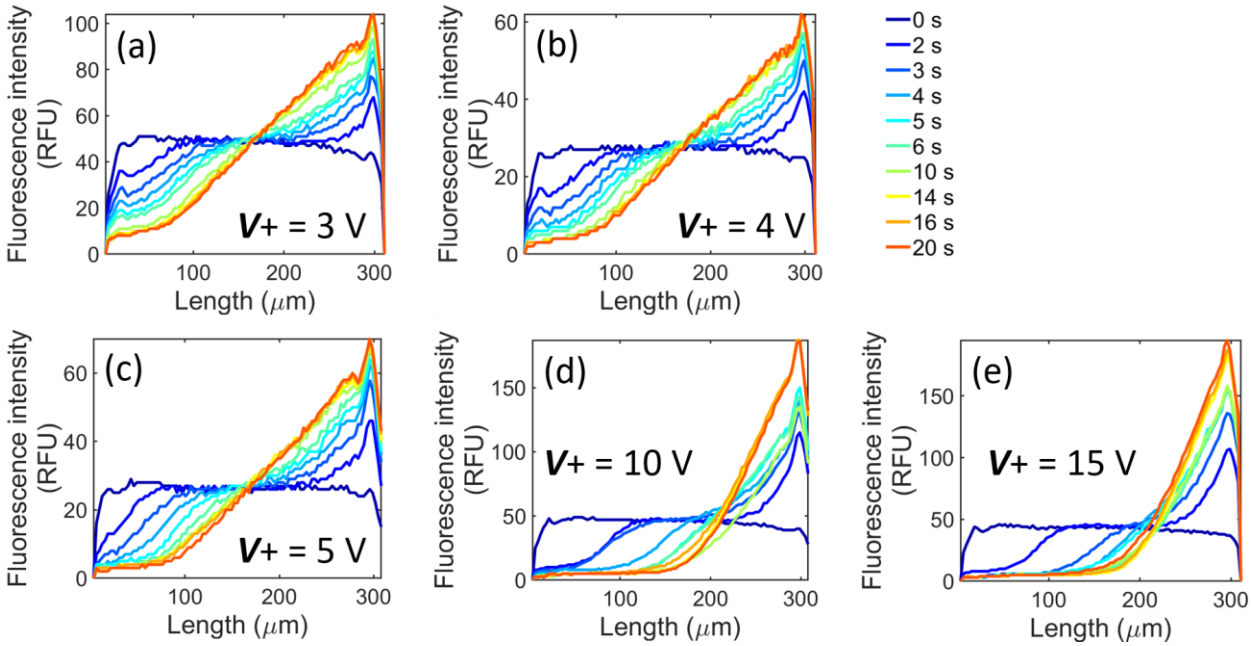

Fig. S5. Temporal evolution of the fluorescence intensity profile along the droplet centerline of a 4.6 nL droplet containing 10.0 mM phosphate buffer and 10.0 μM $BODIPY^{2-}$. The applied voltage bias was (a) 3.0 V, (b) 4.0 V, (c) 5.0 V, (d) 10.0 V, and (e) 15.0 V.

In-droplet separation of analytes with distinct electrophoretic mobilities. Figure S6 shows the results obtained during in-droplet ICP of two anionic tracers having higher ($BODIPY^{2-}$, green) and lower (Texas Red, red) mobility, relative to each other. In this experiment, stationary droplets comprising 10.0 µM $BODIPY^{2-}$, 100 µM Texas Red, and 90.0 mM phosphate buffer (pH 7.3) were subjected to $V+$ = 100 V (**Figure S6a,b,c,d**), and 150 V (**Figure S6e,f,g,h**), and images of green (**Figure S6b,f**) and red (**Figure S6c,g**) fluorescence were obtained after 10 s. An overlay of the brightfield images of each droplet with red and green fluorescence (**Figure S6a,e**) show three distinct regions - depletion of both dyes (bottom, cathodic end), red dye only (middle), and both dyes together (top, anodic end).

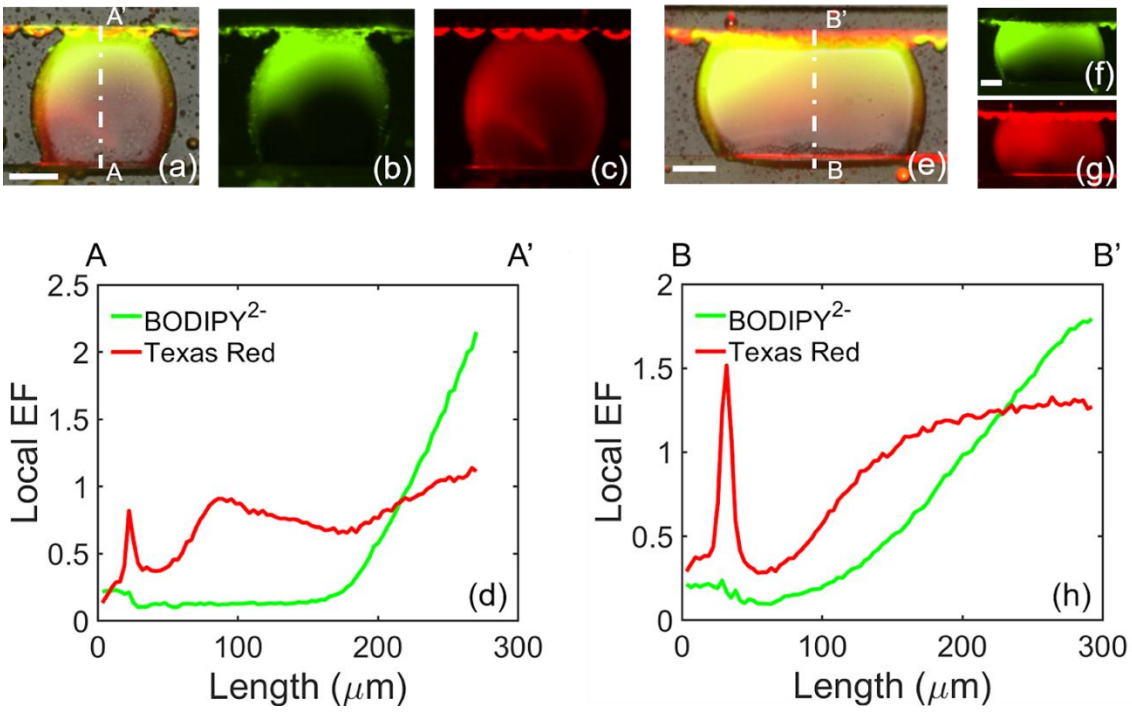

Fig. S6. In-droplet separation of analytes with distinct electrophoretic mobilities. (a and e) Overlaid of brightfield images with the fluorescence images showing the distributions of the (b and f) green tracer ($BODIPY^{2-}$) and (c and g) red tracer (Texas Red). Both droplets contained 90.0 mM phosphate buffer (pH 7.3), 10.0 μM $BODIPY^{2-}$, and 100 μM Texas Red. The droplet volumes were (a-d) 2.7 nL and (e-h) 6.6 nL, for which voltage biases were $V+$ = 100 V and 150 V, respectively. The scale bar is 100 μm. (d and h) Plots of the local degree of enrichment (local EF), along the cutlines (A-A', B-B') indicated in (a) and (d).

Cation transport into droplets. Figure S7 shows fluorescence images of the same set of three W/O droplets obtained over the time course of two successive experiments. Initially, the droplets contained 10.0 μM Rhod-2 calcium indicator dye in 10.0 mM Tris buffer. In a first experiment (right column of images) both auxiliary channels were filled with 10.0 mM Tris buffer. A voltage bias of 10.0 V was applied, and fluorescence images were obtained immediately and then at t = 10, 20, and 30 min thereafter. At t = 30 min, the voltage bias was removed, and after waiting 5 min to allow redistribution of the dye, an additional image was obtained. In a second experiment (left column of images), the solution in the anodic auxiliary was replaced with 10.0 mM $CaCl_2$. An identical voltage and image program was repeated. The fluorescence intensity of the indicator dye is increased only in the presence of $CaCl_2$. Further, the size of the IDZ is decreased in the presence of $CaCl_2$, which is attributed to decreased mobility of the indicator upon binding Ca^{2+}.

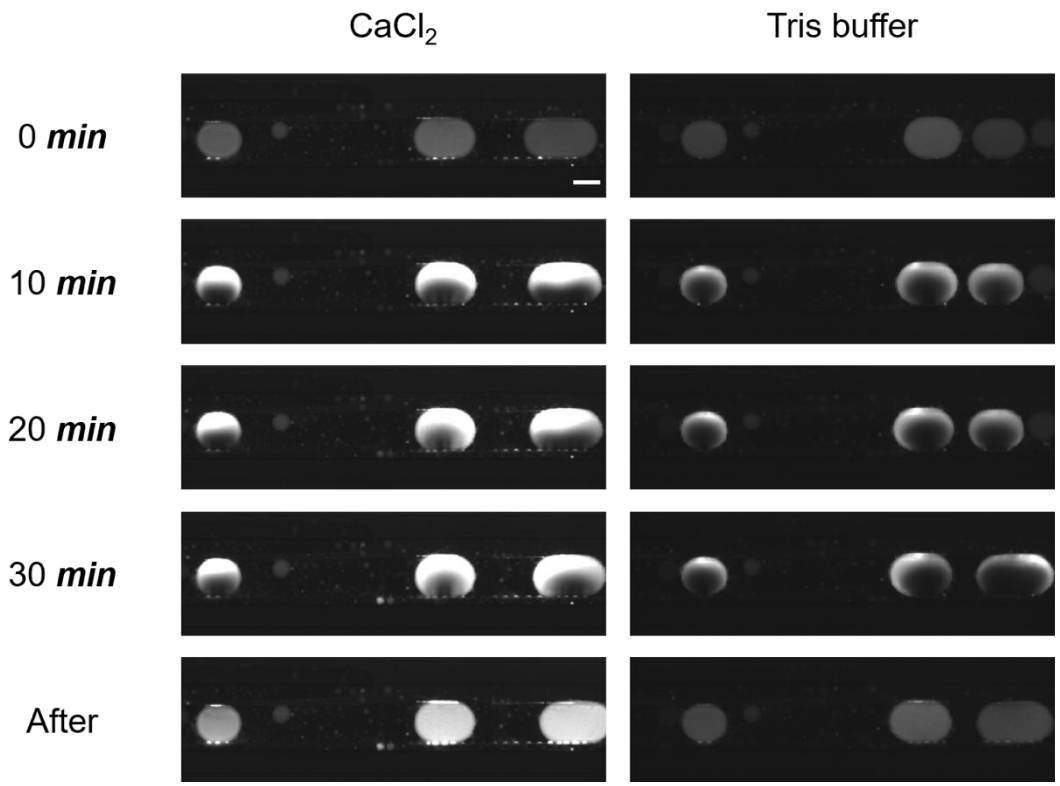

Fig. S7. Calcium injection from the auxiliary channel to the droplets. Initially, the droplet contained 10.0 mM Tris buffer and 10 μM of the calcium indicator, Rhod-2. In two successive experiments, the anodic auxiliary channel contained, first, 10.0 mM Tris buffer (right column) and 10.0 mM $CaCl_2$ (left column). In each case, following initiation of $V+ = 10.0$ V at $t = 0$ s, fluorescence images were obtained at the times indicated. An additional image was obtained 5 min after removal of the voltage bias ('After') to allow the indicator dye to become uniformly distributed.

SI References

1. Yu, M.; Hou, Y.; Zhou, H.; Yao, S. An on-demand nanofluidic concentrator. *Lab Chip* **2015**, *15*, 1524–1532.
2. Chen, C.-H.; Sarkar, A.; Song, Y.-A.; Miller, M. A.; Kim, S. J.; Griffith, L. G.; Lauffenburger, D. A.; Han, J. Enhancing Protease Activity Assay in Droplet-Based Microfluidics Using a Biomolecule Concentrator. *J. Am. Chem. Soc.* **2011**, *133*, 10368–10371.
3. Sanghavi, B. J.; Varhue, W.; Chávez, J. L.; Chou, C.-F.; Swami, N. S. Electrokinetic preconcentration and detection of neuropeptides at patterned graphene-modified electrodes in a nanochannel. *Anal. Chem.* **2014**, *86*, 4120–4125.
4. Petersson, M.; Nilsson, J.; Wallman, L.; Laurell, T.; Johansson, J.; Nilsson, S. Sample enrichment in a single levitated droplet for capillary electrophoresis. *J. Chrom. B: Biomed. Sci. Appl.* **1998**, *714*, 39–46.
5. He, M.; Sun, C.; Chiu, D. T. Concentrating solutes and nanoparticles within individual aqueous microdroplets. *Anal. Chem.* **2004**, *76*, 1222–1227.
6. Park, K.; Park, J; Jung, J. H.; Destgeer, G.; Ahmed, H.; Sung, H. J. In-droplet microparticle separation using travelling surface acoustic wave. *Biomicrofluidics* **2017**, *11*, 064112.